Nuclear Acoustic Resonance of Mn^{55} in Antiferromagnetic $RbMnF_3$ †

J. B. Merry* and D. I. Bolef
Arthur Holly Compton Laboratory of Physics, Washington University, St. Louis, Missouri 63130
(Received 2 February 1971)

An intense frequency-dependent absorption of ultrasound in antiferromagnetic $RbMnF_3$ has been observed and attributed to resonant phonon coupling to the manganese nuclear spins. At 4.2 K, the maximum resonant absorption using longitudinal waves at $\nu = 650$ MHz was much greater than 40 dB/cm and was accompanied by a dispersion (shift in acoustic velocity) of greater than 1%. Both the field-dependent and field-independent modes, with the electronic spins in a flopped configuration, have been studied. The observed nuclear acoustic resonance absorption and dispersion are well accounted for by the magneto-elastic theory of Fedders. A semiclassical model of the magneto-elastic theory, which agrees in most respects with that of Fedders, is described. It is shown further that this model can be extended to explain the coupling of ultrasound to the nuclear spins of magnetic atoms (e.g., Mn^{55} in MnTe) and nonmagnetic atoms (e.g., F^{19} in $RbMnF_3$) in other antiferromagnets.

I. INTRODUCTION

The strong resonant interaction of ultrasound with both the field-dependent and field-independent Mn^{55} nuclear acoustic resonance (NAR) modes in the cubic antiferromagnet $RbMnF_3$ has been observed by the present authors[1,2] and by Platzker and Morganthaler.[3] The nuclear acoustic resonance of Mn^{55} in antiferromagnetic MnTe has been reported by Walther.[4,5] A detailed theory of the interaction of acoustic phonons with the coupled system of electronic and nuclear spins in a cubic antiferromagnet, with particular reference to $RbMnF_3$, has been given by Fedders.[6] In this theory, the mechanism coupling the nuclear spins and the phonons is a magneto-elastic one, first proposed by Silverstein[7] in his theory of NAR in uniaxial antiferromagnets. Another mechanism for the Mn^{55} spin-phonon coupling has been proposed by Shrivastava and Stevens.[8]

In this paper, we present a more detailed report of experimental studies of Mn^{55} NAR and of electronic spin-phonon coupling in $RbMnF_3$ in the ultra-high-frequency (uhf) region. We present results on both the field-dependent and field-independent Mn^{55} nuclear resonance modes, and compare these results with the predictions of theory. Excellent agreement is found with the magneto-elastic theory of Fedders. In Sec. II, we propose a semiclassical model which is then utilized to derive the angular dependence of the magneto-elastic interaction. In this section, we also write the equilibrium conditions for the sublattice magnetization in a convenient general form. The experimental results obtained from acoustic absorption and dispersion measurements made in the uhf region are presented in Sec. III. In Sec. IV, we interpret these results and compare them in detail with the predictions of the magneto-elastic theory. In Sec. V, we show that this magneto-elastic NAR theory can be extended to the nuclei of other antiferromagnets (e.g., Mn^{55} in MnTe and F^{19} in $RbMnF_3$).

II. THEORY OF NUCLEAR SPIN-PHONON COUPLING IN $RbMnF_3$

A. Magnetic Properties of $RbMnF_3$

$RbMnF_3$ is a cubic antiferromagnet with a Néel temperature T_N of 83 K. The magnetic properties of this antiferromagnet can largely be described in terms of internal fields: the anisotropy field H_A, the hyperfine field H_N, the nuclear polarization field H_{NE}, and the exchange field H_E. The anisotropy field is strongly dependent upon crystalline impurities; H_A has been observed to vary from 4.59 to 0 Oe as cobalt doping was increased from 0 to 620 ppm.[9] Even in crystals grown without intentional impurities, H_A has been found to vary from 3 to 4.59 Oe.[10–12] The hyperfine field $\vec{H}_N$ is parallel to the sublattice magnetization $\vec{M}_0$. The hyperfine frequency $\nu_N = \gamma_N H_N / 2\pi = 686.2$ MHz at 4.2 K; γ_N is the nuclear gyromagnetic ratio for Mn^{55}. The Mn nuclear polarization field seen by the electrons is $H_{NE} = (9.43/T)$ Oe and is also parallel to $\vec{M}_0$.[13] The exchange field as determined by Ince[10] is $H_E = 0.816 \times 10^6$ Oe for $T = 4.2$ K.

The calculated magnitude of the sublattice magnetization M_0 for each sublattice is 305 Oe at the zero-temperature limit where the thermal average of the electronic spins $\langle \vec{S} \rangle = \frac{5}{2}$. The orientation of the sublattice magnetization is essentially perpendicular to the applied field $\vec{H}_0$ when $H_0 > (2H_E H_A)^{1/2}$ (~ 2 kOe). When in this spin-flopped state, the magnetization $\vec{M}_0$ is canted toward $\vec{H}_0$ by a small angle $t = H_0 / 2H_E$. All measurements reported in Sec. III were taken in the spin-flopped state.

$RbMnF_3$ has been the object of extensive studies of Mn^{55} nuclear magnetic resonance (NMR) and antiferromagnetic resonance (AFMR).[10,13-16] The strong hyperfine field in $RbMnF_3$ puts the nuclear resonance frequency in the uhf region; the small anisotropy field puts the AFMR frequency in the X-band microwave region. The combination of small H_A and large hyperfine constant A causes these nuclear and electronic modes to be strongly coupled. This strong electron-nuclear coupling gives rise to a large frequency pulling of the nuclear modes by the electronic modes. As for any antiferromagnet in a spin-flopped configuration, $RbMnF_3$ has two nondegenerate AFM modes. The resonance frequencies of the field-dependent (ω_{e+}) and the field-independent (ω_{e-}) antiferromagnetic modes are given by[13,15]

$$\omega_{e+} = \gamma_e (H_0^2 + 2H_E H_{NE} + 3BH_E H_A)^{1/2} , \tag{1a}$$

$$\omega_{e-} = \gamma_e (2H_E H_{NE} + 3CH_E H_A)^{1/2} , \tag{1b}$$

where γ_e is the electronic gyromagnetic ratio, and B and C are functions of the orientation of $\vec{H}_0$. The coupling of these AFM modes to the nuclei gives rise to two nondegenerate nuclear modes whose resonance frequencies are given by[16]

$$\omega_{n\pm} = \omega_N [1 - 2\gamma_e^2 H_E H_{NE} / (\omega_{e\pm})^2]^{1/2} , \tag{2}$$

where ω_N ($=\gamma_n H_N$) is the unpulled Mn^{55} resonance frequency. The ω_{n+} mode is field dependent and the ω_{n-} mode is field independent. Only the ω_{n+} mode has been observed by NMR with the spins in a flopped configuration.[16,17] Further information on the properties of $RbMnF_3$ and its magnetic modes can be found in the doctoral dissertations of Melcher[18] and of Ince.[19]

B. Rigorous Magnetoelastic Theory of Spin-Phonon Coupling

In the magneto-elastic theory of Fedders,[6] coupling of ultrasound to the coupled system of electronic and nuclear spins proceeds via a modulation of the effective anisotropy field. This modulation causes a rocking of the sublattice magnetization, resulting finally in a coupling of energy to the nuclei via the hyperfine field. Fedders has applied this theory to calculate the acoustic dispersion and absorption in a cubic antiferromagnet. For a flopped spin configuration, and for $|\omega - \omega_n|$ and $|\omega - \omega_e|$ much greater than the nuclear and antiferromagnetic linewidths, respectively, the calculated acoustic dispersion is given by

$$\Delta\omega_{\pm}(\mathrm{sec}^{-1}) = \frac{2b_1^2\gamma_e}{\rho M_0 v^2}\,\omega_E\,\omega \times \left[\frac{2\omega_E\,\omega_{NE}\,\omega_N^2}{\omega_{e\pm}^4(\omega^2 - \omega_{n\pm}^2)} + \frac{1}{\omega^2 - \omega_{e\pm}^2}\right]\Gamma_{\pm} , \tag{3}$$

where $\Gamma_{\pm}$ is a function dependent only on the orientation of $\vec{H}_0$ for a given acoustic propagation vector $\vec{k}$, ρ is the density, v is the acoustic velocity, b_1 is a magneto-elastic coupling constant, $\omega_E = \gamma_e H_E$, and $\omega_{NE} = \gamma_e H_{NE}$. This calculation was made considering longitudinal waves propagating along a cube axis. The first term in the brackets is due to the nuclear spin-phonon interaction via the electrons; the second term is due solely to an electronic spin-phonon interaction. The corresponding NAR absorption near nuclear resonance is given by

$$\alpha_{\pm} = \frac{2\pi\gamma_e\,\omega_E^2\omega_{NE}\,\omega_N}{\rho v^2 M_0\,\omega_{e\pm}^4}\left(\frac{\omega_N}{\omega_{n\pm}}\right) b_1^2\,\Gamma_{\pm} g(\omega) , \tag{4}$$

where $g(\omega)$ is the Lorentzian line-shape function. This magneto-elastic theory is more than a theory of *nuclear* acoustic resonance. The contribution from the antiferromagnetic modes in the uhf region can be comparable to the nuclear acoustic dispersion.

C. Semiclassical Model of Mn^{55} NAR

Results similar to those reported by Fedders can be obtained from a semiclassical calculation similar to that suggested in Silverstein's paper.[7] Although the method is less general than that used by Fedders, it gives physical insight into the coupling mechanism and aids in the construction of a simple model. Using this model, the angular function $\Gamma_{\pm}$ can be readily calculated for arbitrary field configurations. The nuclear spin-phonon interaction is treated in terms of an effective rf field $\vec{H}_1$ (perpendicular to I_z) interacting with the nuclear dipole moment. The interaction Hamiltonian is then

$$\mathcal{H}_I = \gamma_n \hbar \vec{I} \cdot \vec{H}_1 = \tfrac{1}{4}\gamma_n \hbar H_1 (I_+ e^{-i\omega t} + I_- e^{+i\omega t}) , \tag{5}$$

where H_1 is the field produced by time-dependent crystalline strains e_{ij} (ultrasonic waves). Following a standard perturbation treatment, one can derive an acoustic absorption coefficient α_n (in units of rad/sec)[20,21]:

$$\alpha_n(\mathrm{sec}^{-1}) = \frac{\pi N \hbar \omega \gamma_n^2 H_1^2 \langle I \rangle}{4\rho v^2 e_{ij}^2} g(\omega) , \tag{6}$$

where N is the number of spins and $\langle I \rangle$ is the thermal average of the spin angular momentum.

An expression for H_1 may be obtained by noting that the presence of ultrasonic strains gives rise to an effective magneto-elastic field $\vec{H}_{ME}$ given by

$$\vec{H}_{ME} = \nabla_{\vec{M}} E_{ME} , \tag{7}$$

where[22]

$$E_{ME} = \frac{b_1}{M_0^2}\sum_{i=1}^{3} M_i^2 e_{ii} + \frac{b_2}{M_0^2}\sum_{i>j} M_i M_j e_{ij} . \tag{8}$$

The nuclei, however, see a field much larger than $\vec{H}_{ME}$. As in the case for Mn NMR in $RbMnF_3$,[16] there is a large enhancement of the induced rf field

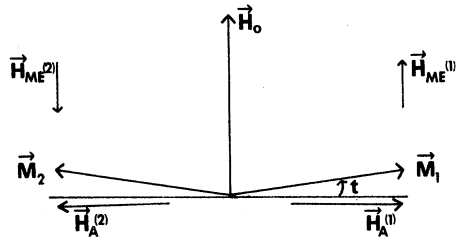

FIG. 1. Electronic (+) mode ω_{e+} excited by a magneto-elastic field H_{ME} in a spin-flopped antiferromagnet. t ($\sim 0.2°$) is the tilt angle of $\vec{M}$, and (1) and (2) indicate the different magnetic sublattices.

by the electrons. The time-dependent field seen by the nuclei comes from a magneto-elastic modulation of a large hyperfine field. The details of the model are most easily derived for a spin-flopped uniaxial antiferromagnet, schematically shown in Fig. 1. The results are readily extended to a cubic antiferromagnet. It is convenient at this point to introduce a new quantity, H_c, the constraining field. The sublattice magnetization is constrained to its equilibrium configuration by the components of the internal field $\vec{H}_A$ and the applied field $\vec{H}_0$ that are parallel to $\vec{M}_0$; this field will be called the constraining field. If a magneto-elastic field $\vec{H}_{ME}$ perturbs the sublattice magnetization as shown in Fig. 1, then $\vec{M}_0$ would rock through an angle β given by $\beta = H_{ME}/H_c$. The effective field $\vec{H}_{ME}$ perpendicular to $\vec{M}_0$ excites the electronic modes. Consider, for example, the effect of a component of $\vec{H}_{ME}$ parallel to $\vec{H}_0$ as shown in Fig. 1. This configuration of $\vec{H}_{ME}$ causes the sublattice to gyrate about an axis perpendicular to the plane of the figure. The constraining field is then

$$H_c(+) = H_A + H_0 \sin t = H_A + \frac{H_0^2}{2H_E} = \frac{\omega_{e+}^2}{2\gamma_e \omega_E} , \quad (9)$$

where $\omega_{e+} = \gamma_e (H_0^2 + 2H_E H_A)^{1/2}$, the frequency of the field-dependent mode for a uniaxial antiferromagnet. A component of $\vec{H}_{ME}$ perpendicular to $\vec{H}_0$ and $\vec{M}_0$, on the other hand, causes the sublattice magnetization to gyrate about an axis parallel to $\vec{H}_0$. The constraining field in that case is

$$H_c(-) = H_A = \omega_{e-}^2 / 2\gamma_e \omega_E , \quad (10)$$

where $\omega_{e-} = \gamma_e (2H_E H_A)^{1/2}$, the frequency of the field-independent mode for a uniaxial antiferromagnet. Equations (9) and (10) can be extended to apply to a cubic antiferromagnet by using the definitions of $\omega_{e\pm}$ given in Eq. (1). The constraining field may always be found from the equation for the antiferromagnetic resonance frequency since, in general, $(\omega_e/\gamma_e)^2 = 2H_E H_c$.

The perturbing field is given by

$$H_1(\pm) = H_N \tan\beta = \frac{2AS\gamma_e \omega_E}{\hbar \gamma_n \omega_{e\pm}^2} \vec{H}_{ME} \cdot \hat{\epsilon}_\pm , \quad (11)$$

where $\hat{\epsilon}_+ = \vec{H}_0/|\vec{H}_0|$ and $\hat{\epsilon}_- = \vec{M}_0 \times \vec{H}_0 / |\vec{M}_0|\,|\vec{H}_0|$. The acoustic attenuation can now be written as

$$\alpha_n = \frac{\pi N \hbar \omega}{4\rho v^2 M_0^2} \left(\frac{2AS\gamma_e \omega_E}{\hbar \omega_{e\pm}^2} \right)^2 B_\pm^2 \Gamma_\pm \langle I \rangle g(\omega) , \quad (12)$$

where we have set $(\vec{H}_{ME} \cdot \hat{\epsilon}_\pm)^2 = B_\pm^2 \Gamma_\pm e_{ij}^2 / M_0^2$. Using conventional definitions of H_N, H_{NE}, and M_0, the acoustic attenuation can be written in a form similar to that of Fedders [Eq. (4)][21]:

$$\alpha_n = \left[\frac{2\pi\gamma_e}{\rho v^2 M_0} \frac{\omega_E^2 \omega_{NE} \omega_N \omega}{\omega_{e\pm}^4} g(\omega) \right] B_\pm^2 \Gamma_\pm . \quad (13)$$

If $g(\omega)$ is replaced by a Lorentzian line for which $|\omega - \omega_n|$ is much greater than the nuclear linewidth, then Eq. (13) and Fedders's expression differ only by a factor of ω_N/ω_n. This difference arises because the correlation of nuclear and electronic spins was not considered here as it was in Fedders's derivation. The NAR coupling to the nuclear spin of the magnetic atom described by Eq. (13) is basically the same for any antiferromagnet. Only the angular dependence $B^2\Gamma$ and the exact form of ω_e depend on lattice symmetry. Silverstein's equation for a uniaxial antiferromagnet,[7] for example, can be shown to be identical to Eq. (13).

Using the present semiclassical model, the NAR coupling described by Eq. (13) can be interpreted as resulting from the excitation of the nuclear mode ω_{n+} (ω_{n-}) via the corresponding electronic mode ω_{e+} (ω_{e-}). The magneto-elastic field that couples to the electronic magnetization differs in sign at different sublattices. The electronic mode is thus excited by the component of $\vec{H}_{ME}$ parallel to the major axis of precession of the mode. From these considerations, it can be seen that the NAR interaction should be strong for *both* nuclear modes. Nuclear magnetic resonance, on the other hand, is observable only for the ω_{n+} mode in the spin-flopped regime.

D. NAR Angular Dependence and Equilibrium Conditions

The angular dependence $B^2\Gamma$ of the interaction may be evaluated explicitly by using Eqs. (7), (8), and the expressions for $\hat{\epsilon}_+$ and $\hat{\epsilon}_-$ given above. The angular factor is a function of the three angles shown in Fig. 2. The position of $\vec{H}_0$ in a given plane is specified by the angle ψ, and the position of $\vec{M}_0$ is specified by θ and ϕ. It is more convenient to write the angular dependence in terms of a single experimentally measurable angle, ψ. To express θ and ϕ in terms of ψ, the magnetization equilibrium conditions are needed. We derive the equilibrium conditions for the spin-flopped case for $\vec{H}_0$ anywhere in the (100) and (1$\bar{1}$0) planes.

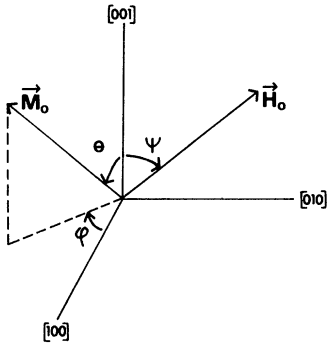

FIG. 2. Spherical angles used to describe the orientation of the applied field $\vec{H}_0$ and the sublattice magnetization $\vec{M}_0$.

These conditions have been given previously for $\vec{H}_0$ along three discrete directions.[11]

When the electron spins are completely flopped, the electronic magnetizations lie in a plane perpendicular to $\vec{H}_0$, and their position in that plane is determined solely by the anisotropy energy[22]:

$$E_A = (K/M_0^4)(M_x^2M_y^2 + M_y^2M_z^2 + M_z^2M_x^2) , \qquad (14)$$

where K is the anisotropy constant for cubic $RbMnF_3$. The coordinates x, y, and z are coincident with the [100], [010], and [001] crystal axes, respectively. The equilibrium conditions are most easily determined by specifying the spin orientation with respect to a transformed coordinate system with the z' axis parallel to $\vec{H}_0$, in which case $\theta' = 90°$ and ϕ' is the only variable. The equilibrium condition in the transformed system for $\vec{H}_0$ in the (100) plane is[21]

$$\frac{\partial E_A(\psi, \phi')}{\partial \phi'} = (4 - \sin^2 2\psi)\sin^2\phi' - 2 = 0 . \qquad (15)$$

For $\vec{H}_0$ in the $(1\bar{1}0)$ plane, the equilibrium condition is[21]

$$\sin 2\phi' \left\{ \begin{matrix} \sin^2\phi'(1 + 4\cos^2\psi - 3\cos^4\psi) \\ + 2\cos 2\phi'(1 - \tfrac{3}{2}\cos^2\psi) - 1 \end{matrix} \right\} = 0 . \qquad (16)$$

For $0 \le \psi \le 54.7°$ with $\vec{H}_0$ in the $(1\bar{1}0)$ plane, the stable equilibrium condition is given by $\sin 2\phi' = 0$, i.e., $\theta = 90 + \psi$. For $54.7 \le \psi \le 180 - 54.7$, the bracketed factor gives the stable solution.

Using these equilibrium conditions and the associated transformation equations, the angular dependence $B_\pm^2\Gamma_\pm$ can be written in the form shown in Table I. The symbol $\hat{e}$ denotes the direction of polarization of the acoustic wave.

III. EXPERIMENT

A. Experimental Techniques

The specimen of $RbMnF_3$ used in this study was the same as that used by Melcher and Bolef in their study of F^{19} NAR.[12] The crystal (S3A by their designation) was cut and polished so that the ultrasonic propagation vector $\vec{k}$ was parallel to a cube edge. We choose $\vec{k} \parallel [001]$. To generate longitudinal ultrasonic waves, cadmium sulfide piezoelectric transducers were evaporated onto the plane parallel faces of the crystal. Changes in velocity and attenuation were measured by means of a sampled-cw transmission spectrometer. This technique has been described in detail by Miller and Bolef.[23] The data were taken with $T \simeq 4$ K and $H_0 > (2H_E H_A)^{1/2}$.

B. NAR Absorption

Both the field-dependent (+) and the field-independent (−) nuclear modes were observed to give rise to an extraordinarily intense acoustic absorption at resonance. The intensity of the absorption rendered unnecessary the use of the usual sensitive NAR detection techniques. For $\vec{H}_0$ along a cube axis, the NAR absorption vanished. As ψ increases, the absorption increases markedly, from approximately 6 dB/cm for $\psi = 1°$ to 30 dB/cm for $\psi = 10°$. For $\psi = 45°$, the NAR absorption was a maximum and was so intense that the swept frequency pattern was obliterated.[1] The absorption at the center of the resonance was too great to be measured easily. Measurements in the wings of the (+) mode showed that the maximum attenuation was much greater than 40 dB/cm.

The field dependence of the NAR frequency ν_{n+} is shown (solid dots) in Fig. 3 for $T = 4.20$ K, $\psi = 0.3°$, and $\vec{H}_0$ in the (100) plane. For $\nu = 662.27$ MHz, $\psi = 0.7°$, and $T = 4.8$ K, the field at the center of the (+) mode absorption line was 6.857 kOe and the field width at the half-power points was 56 Oe. The line shape of the (−) mode (data not shown) was

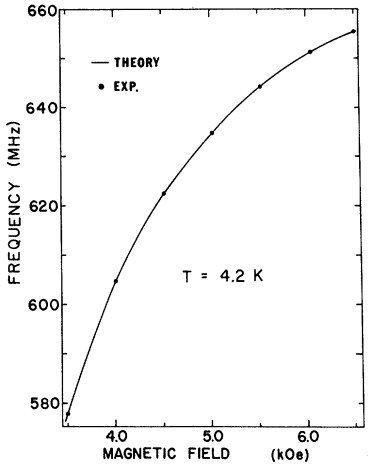

FIG. 3. Nuclear acoustic resonance frequency ν_{n+} versus the applied field H_0. $\vec{H}_0$ is in the (100) plane, $\psi = 0.3°$.

determined by measuring the difference in power absorption for $\psi = 0°$ and $\psi = 10°$. Since the NAR absorption was observed to vanish for $\psi = 0°$, the difference of the power absorption at the two angles was attributed to NAR. The width of the (−) mode NAR line at its half-power points, when $H_0 = 6.00$ kOe, $\psi = 10°$, and $T = 4.3$ K, is approximately 16 ± 3 MHz. The center resonance frequency of this mode was found to be 555 ± 2 MHz.

C. NAR Dispersion

NAR dispersion was measured as a function of frequency and field angle for $\vec{H}_0$ in the $(1\bar{1}0)$ and (100) planes. With the field in the $(1\bar{1}0)$ plane, only the (+) mode was observed when $\psi < 54.7°$. When $\psi \geq 54.7°$, the (−) mode appeared as a strong absorption and dispersion ranging in frequency from 600 MHz to approximately 470 MHz. Hysteresis effects were evident, as previously reported by Teaney *et al.*[13] in their studies of antiferromagnetic resonance. With the field in the (100) plane, the NAR dispersion as a function of frequency was measured near ν_{n+} for $H_0 = 6.00$ kOe and $T = 4.18$ K. The frequencies of several mechanical resonance peaks were measured for $\psi = 0°$ and $\psi = 10.8°$. Since the NAR coupling vanishes for $\psi = 0°$, the dispersion at $\nu(10.8°)$ is given by $\Delta\nu = \nu(10.8°) - \nu(0°)$. Dispersion versus frequency for the ν_{n+} mode is plotted in Fig. 4.

NAR dispersion versus field angle ψ was measured at two frequencies, $\nu(\psi = 0°) = 671.05$ and 599.31 MHz, for $H_0 = 6.00$ kOe and $T = 4.18$ K. Graphs of $\Delta\nu(\psi) \equiv \nu(\psi) - \nu(0°)$ versus ψ at these two frequencies are given in Figs. 5 and 6, respectively.

IV. DISCUSSION

A. Linewidths and Line Shapes

To make meaningful comparisons between theory and experiment, accurate and self-consistent values of ν_N, H_{NE}, H_E, and H_A are needed. The anisotropy field H_A may be obtained from the nuclear resonance frequency data for ν_{n-}. From these data, using Eqs. (2) and (1b), one obtains $H_A = 2.92 \pm 0.05$ Oe. Using this value for H_A, and the values $H_E = 0.810 \times 10^6$ Oe, $H_{NE} = (9.43/T)$ Oe, and $\nu_N = 686.2$ MHz, a theoretical fit of the ν_{n+}-versus-H_0 data shown in Fig. 3 was obtained. The mean deviation between theory and experiment was less than 0.02%.

The field width (δH) and the frequency width ($\delta\nu$) of the (+) mode are not related simply by the nuclear

TABLE I. Angular dependence of the magneto-elastic NAR interaction in a cubic antiferromagnet.

Configuration of $\vec{H}_0$ and $\vec{k}$	$B_+^2\Gamma_+$	$B_-^2\Gamma_-$
$\vec{H}_0$ in (100) $\vec{k}_{long} \parallel$ [001]	$\frac{2b_1^2 \sin^2 2\psi}{4-\sin^2 2\psi}$	$\frac{8b_1^2 (2-\sin^2 2\psi) \sin^4\psi}{(4-\sin^2 2\psi)^2}$
	For $\psi < 54.7°$	
$\vec{H}_0$ in $(1\bar{1}0)$	$b_1^2 \sin^2 2\psi$	0
	For $\psi > 54.7°$	
$\vec{k}_{long} \parallel$ [001]	$\frac{b_1^2(1-3\cos^2\psi) \sin^2 2\psi}{3\cos^4\psi - 10\cos^2\psi + 3}$	$4b_1^2 (1-3\cos^2\psi) \sin^4\psi \times \frac{3\cos^4\psi - 7\cos^2\psi + 2}{(3\cos^4\psi - 10\cos^2\psi + 3)^2}$
$\vec{H}_0$ in (100) $\vec{k}_{long} \parallel$ [011]	$\frac{2b_2^2 \cos^2 2\psi}{4-\sin^2 2\psi}$	$\frac{2(b_1 - b_2 \sin^2 2\psi)^2 (2-\sin^2 2\psi)}{(4-\sin^2 2\psi)^2}$
$\vec{H}_0$ in (100) $\vec{k}_{trans} \parallel$ [001] $\hat{e} \parallel$ [010]	$\frac{2b_2^2 \cos^2 2\psi}{4-\sin^2 2\psi}$	$\frac{2b_2^2 (2-\sin^2 2\psi) \sin^2 2\psi}{(4-\sin^2\psi)^2}$
$\vec{H}_0$ in (100) $\vec{k}_{trans} \parallel$ [001] $\hat{e} \parallel$ [100]	$\frac{b_2^2 (2-\sin^2 2\psi) \cos^2\psi}{4-\sin^2 2\psi}$	$\frac{b_2^2 \cos^4\psi \sin^6\psi}{(4-\sin^2 2\psi)^2}$
	For $\psi < 54.7°$	
$\vec{H}_0$ in $(1\bar{1}0)$ $\vec{k}_{trans} \parallel$ [001] $\hat{e} \parallel$ [110]	$b_2^2 \cos^2 2\psi$	0

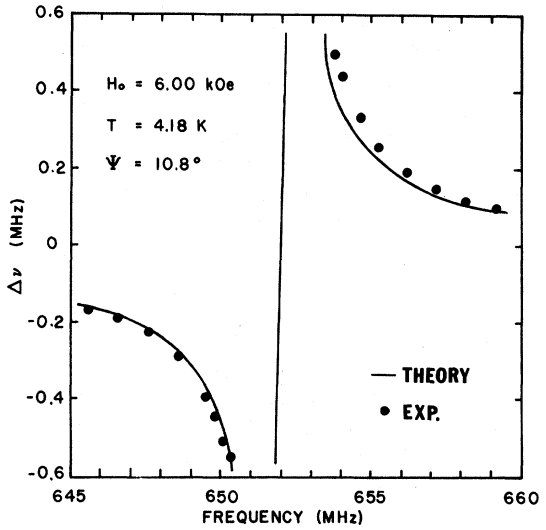

FIG. 4. Calculated and observed dispersion ($\Delta\nu_{n+}$) versus frequency (ν) for $H_0 = 6.00$ kOe and $\vec{H}_0$ in the (100) plane.

gyromagnetic ratio. The field dependence of ν_{n+} comes from the pulling term in Eq. (2): $\nu_{n+} = \nu_N \times [1 - 2H_E H_{NE}/(H_0^2 + 2H_E H_{NE} + 3BH_E H_A)]^{1/2}$. The calculated frequency width of the (+) mode NAR absorption line is $\delta\nu_{n+} = 0.40$ MHz, in agreement with the (+) mode NMR linewidths previously reported.[14,24] The NAR absorption linewidth of the (−) mode is 16 ± 3 MHz, 40 times greater than that for the (+) mode.

The linewidth of the (+) mode in $RbMnF_3$ for $H_0 < 10$ kOe has been partially explained by Weber and Seavey[24] in terms of inhomogeneities in the antiferromagnetic spectrum. They reason that such inhomogeneities, acting through the frequency pulling mechanism, cause a broadening of the nuclear linewidth. Similarly, the large difference between the linewidths of the (+) and (−) NAR modes reported in this work can be explained in terms of an inhomogeneous anisotropy field. Linewidth calculations assuming a ± 0.30 Oe variation of H_A give $\delta\nu_+ = 0.36$ MHz and $\delta\nu_- = 19$ MHz, in good agreement with experiment. The inhomogeneities are attributed to the anisotropy field since H_A has been shown to be strongly dependent upon crystalline impurities.[9]

The NAR absorption line shape is approximately Gaussian. NMR line shapes similar to this have been reported by Weber and Seavey[24] and by Freiser *et al.*[13] NAR dispersion measurements were used to obtain the line shape in the wings, several megahertz away from the center of the resonance line, where inhomogeneous broadening should be absent. The dispersion line shape in this region was found to be Lorentzian. An example is given in Fig. 4, in which the $\Delta\nu_{n+}$-versus-ν data are fitted well by a Lorentzian curve over a range of 8 to 35 half-linewidths. Also, in the following section, good agreement is found between theory and the $\Delta\nu$-versus-ψ data if a Lorentzian line shape is assumed.

B. NAR Intensity and Angular Dependence

The observed intensities of the NAR absorption and dispersion lines are accounted for by the magneto-elastic theory. The peak absorption for the (+) mode was calculated to be 10^3 dB/cm; for the (−) mode, 10^2 dB/cm. In both cases, $H_0 = 6$ kOe. Since measurements of dispersion were more readily and accurately made than those of absorption, quantitative comparison between theory and experiment will be made for both magnitude and angular dependence of the dispersion for four cases.

1. $\Delta\nu$ *versus* ψ; $\vec{H}_0$ *in* (100) *plane and* $\nu(0°) = 671.05$ MHz

In Fig. 5 are shown the values of the dispersion as a function of ψ for the (+) mode (dashed line) and (−) mode (dot-dashed line) calculated for Eq. (3), with the angular dependence taken from row 1 of Table II. The solid line, representing the sum of $\Delta\nu_+$ and $\Delta\nu_-$, shows excellent agreement with the experimental data. The only adjustable parameter in these calculations was b_1, which was set equal to 2.14×10^6 erg/cm^3 for the best fit. This

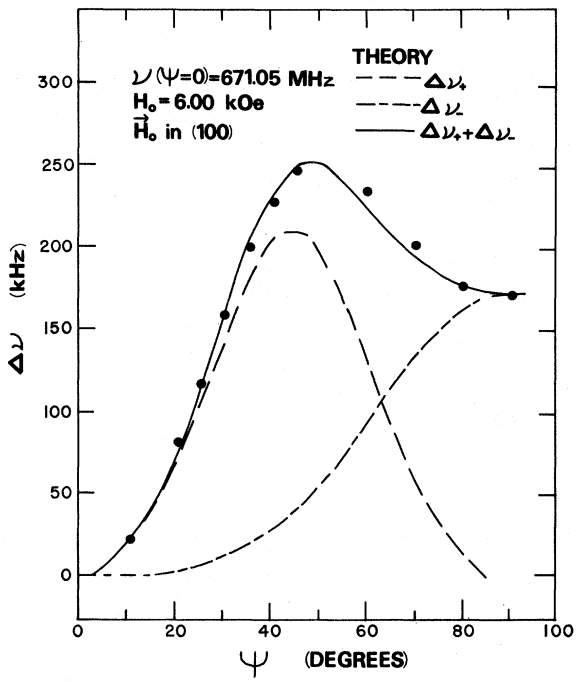

FIG. 5. Calculated and observed dispersion ($\Delta\nu$) versus field angle (ψ) for $H_0 = 6.00$ kOe, $\vec{H}_0$ in the (100) plane, and $\nu(0°) = 671.05$ MHz.

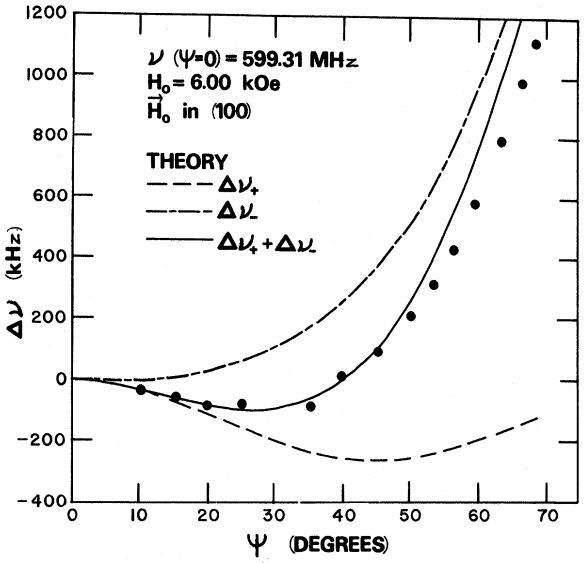

FIG. 6. Calculated and observed dispersion ($\Delta\nu$) versus field angle (ψ) for $H_0 = 6.00$ kOe, $\vec{H}_0$ in the (100) plane, and $\nu(0°) = 599.31$ MHz.

value is close to that $[b_1 = (2.05 \pm 0.05) \times 10^6]$ obtained from the 30-MHz magneto-elastic data of Melcher and Bolef[12] when H_A is assumed to be 2.92 Oe. The data shown in Fig. 5 were taken under conditions such that $\nu_- \cong 540$ MHz and $\nu_+ \cong 655$ MHz, so that $\nu > \nu_{n+}$, $\nu > \nu_{n-}$, and the nuclear dispersion for both modes was positive. The presence of a large negative contribution to the dispersion from both electronic modes is indicated in Fig. 7, in which the dashed line represents the nuclear dispersion $(\Delta\nu_{n+} + \Delta\nu_{n-})$ and the solid line represents the calculated total dispersion. (The solid line in this figure corresponds to that in Fig. 5.)

2. $\Delta\nu$ *versus* ψ; $\vec{H}_0$ *in* (100) *plane and* $\nu(0°) = 599.31$ MHz

In Fig. 6, the calculated total dispersion (solid line), as well as the separate contributions of the (+) mode (dashed line) and the (−) mode (dot-dashed line), is shown. The same value of b_1 (2.14×10^6) as used above was used in these calculations. In the present case, $\nu > \nu_{n-}$ and $\nu < \nu_{n+}$; therefore, the (+) nuclear mode makes a negative contribution to the dispersion. For large angles, the dispersion is determined almost entirely by a positive contribution from the (−) nuclear mode. As can be seen from Fig. 6, the theoretical and experimental curves agree for $\psi < 50°$ but begin to diverge for $\psi > 50°$. This discrepancy may be explained qualitatively by the large linewidth of the (−) mode which limits the accuracy with which ν_{n-} can be measured.

TABLE II. Constants b_1 and H_A for $RbMnF_3$ (specimen S3A).

Source	$b_1(10^6$ erg/cm$^3)$	H_A (Oe)
Mn^{55} NAR data	2.14 ± 0.04	2.92 ± 0.05
30-MHz magneto-elastic data (Ref. 12)	2.05 ± 0.05	3.09 ± 0.20

3. $\Delta\nu$ *versus* ψ; $\vec{H}_0$ *in* $(1\bar{1}0)$ *plane*

For $0° < \psi < 7°$, the observed dispersion (data not shown) in the vicinity of ν_{n+} was found to follow a $\sin^2 2\psi$ dependence as predicted by theory. The (−) mode did not appear until $\psi \gtrsim 54.7°$, also in agreement with theory; i.e., $\Gamma_-(\psi \leq 54.7°) = 0$ and $\Gamma_-(\psi \geq 54.7°) = \sin^4\psi$.

4. $\Delta\nu$ *versus* ν; $\vec{H}_0$ *in* (100) *plane and* $\psi = 10.8°$

The solid line in Fig. 4 represents the dispersion due to the (+) nuclear mode, calculated using Eq. (3) with $\Gamma_+(\psi) = 2\sin^2 2\psi/(4 - \sin^2 2\psi)$. Values of $\psi = 10.8°$ and $b_1 = 2.14 \times 10^6$ erg/cm^3 were used in this calculation.

As shown in Table II, the values of b_1 and H_A obtained in the present work are in good agreement with those calculated from the 30-MHz magneto-elastic data of Melcher and Bolef.[12]

V. CONCLUSIONS

The Mn^{55} NAR data of $RbMnF_3$ reported in this

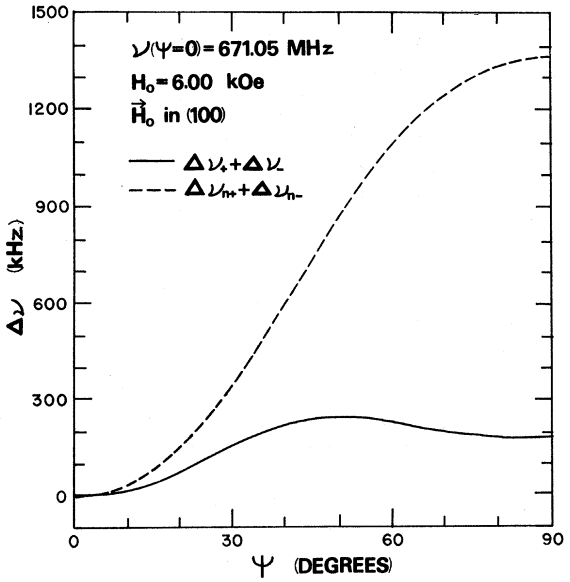

FIG. 7. Calculated acoustic dispersion versus field angle. The solid line represents the sum of nuclear and electronic dispersion $\Delta\nu$; the dashed line represents the nuclear dispersion $\Delta\nu_n$ only.

paper are in excellent agreement with the predictions of the magneto-elastic theory. The semiclassical model discussed above suggests that the magneto-elastic NAR theory may be generalized to apply to the nuclei of magnetic and nonmagnetic atoms in any antiferromagnet. Equation (13) for the NAR absorption of the nuclei in an antiferromagnet may be rewritten so as to indicate more explicitly the dependence of α_n on ν_n and H_A (Ref. 21):

$$\alpha_n(\mathrm{sec}^{-1}) = \frac{2\pi^3 \hbar I(I+1)}{\rho M_0 v^2 \gamma_e \langle S \rangle 3kT} \frac{B^2 \nu_N^4}{H_c^2} \Gamma g(\nu) . \quad (17)$$

In deriving this equation, it has been assumed that the pulling of the nuclear frequency is negligible and that H_N is much larger than any applied field. For many antiferromagnets, including $RbMnF_3$, the constraining field H_c is approximately equal to the anisotropy field H_A. From Eq. (17), the extraordinarily large NAR attenuation of Mn^{55} in $RbMnF_3$ may be attributed to the high nuclear resonance frequency ($\nu_N = 650-680$ MHz) and to the small anisotropy field (the effective anisotropy field at 4.2 K is ~6 Oe). Indeed, any antiferromagnet which contains Mn^{55} and has a small anisotropy field ($H_A \lesssim 300$ Oe) should exhibit a strong nuclear acoustic resonance ($\alpha_n = 10-10^4$ dB/cm). Among the materials which have these properties are MnTe, $KMnF_3$, and $CsMnF_3$.

A strong Mn^{55} NAR absorption has been observed by Walther in MnTe.[4,5] This large NAR signal has several properties which indicate that the magneto-elastic interaction is responsible for it. The frequency dependence ($\alpha_n \sim \nu_N^4$) and the field dependence of the NAR attenuation reported by Walther are in agreement with predictions of the magneto-elastic theory.[21] The observed NAR attenuation ($\alpha_n = 290$ dB/cm for $\nu_N = 398$ MHz, $T = 187$ K, $H_0 = 0$) agrees with that calculated[21] using estimated values of the nuclear linewidth $1/T_2$, H_A, and B: $1/T_2 \cong 1$ MHz,[24] $H_A(187\ \mathrm{K}) \cong 7$ Oe,[25] and $B \cong 3.5 \times 10^6$ erg/cm^3.[21]

The semiclassical model of the magneto-elastic theory has been extended to explain the coupling of ultrasound to the nuclei of nonmagnetic atoms.[21,26] Specifically, it has been shown that the (−) mode of the magneto-elastic interaction can account for the F^{19} NAR in $RbMnF_3$ if the symmetry of the fluorine site is broken.

ACKNOWLEDGMENTS

We acknowledge with gratitude the contributions of our colleagues, P. A. Fedders and J. G. Miller, to all aspects of this work.

---

†Sponsored in part by the National Science Foundation.

*Present address: Air Force Cambridge Research Labs, Bedford, Mass.

[1]J. B. Merry and D. I. Bolef, Phys. Rev. Letters 23, 126 (1969).

[2]J. B. Merry and D. I. Bolef, J. Appl. Phys. 41, 1412 (1970).

[3]A. Platzker and F. R. Morganthaler, Phys. Letters 30A, 515 (1969).

[4]K. Walther, Solid State Commun. 5, 399 (1967).

[5]K. Walther, Phys. Letters 32A, 201 (1970).

[6]P. A. Fedders, Phys. Rev. B 1, 3756 (1970).

[7]S. D. Silverstein, Phys. Rev. 132, 997 (1963).

[8]K. N. Shrivastava and K. W. H. Stevens, J. Phys. C 3, 164 (1970).

[9]W. J. Ince, D. Gabbe, and A. Linz, Phys. Rev. 185, 482 (1969).

[10]W. J. Ince, Phys. Rev. 184, 574 (1969).

[11]P. H. Cole and W. J. Ince, Phys. Rev. 150, 377 (1966).

[12]R. L. Melcher and D. I. Bolef, Phys. Rev. 186, 491 (1969).

[13]D. T. Teaney, M. J. Freiser, and R. H. W. Stevenson, Phys. Rev. Letters 9, 212 (1962).

[14]M. J. Freiser, R. J. Joenk, P. E. Seiden, and D. T. Teaney, in *Proceedings of the International Conference on Magnetism, Nottingham*, 1964 (The Institute of Physics and the Physical Society, London, 1965), p. 432.

[15]M. J. Freiser, P. E. Seiden, and D. T. Teaney, Phys. Rev. Letters 10, 293 (1963).

[16]A. J. Heeger and D. T. Teaney, J. Appl. Phys. 35, 846 (1964).

[17]W. J. Ince and F. R. Morganthaler, Phys. Letters 29A, 106 (1969).

[18]R. L. Melcher, Ph. D. thesis (Washington University, 1968) (unpublished).

[19]W. J. Ince, Ph. D. thesis (Massachusetts Institute of Technology, 1969) (unpublished).

[20]D. I. Bolef, in *Physical Acoustics*, edited by W. P. Mason (Academic, New York, 1966), Vol. 4A, Chap. 3.

[21]J. B. Merry, Ph. D. thesis (Washington University, 1970) (unpublished).

[22]J. Kanamori, in *Magnetism*, edited by G. T. Rado and H. Suhl (Academic, New York, 1963), Vol. 1, Chap. 4.

[23]J. G. Miller and D. I. Bolef, Rev. Sci. Instr. 40, 915 (1969).

[24]R. Weber and M. H. Seavey, Solid State Commun. 7, 619 (1969).

[25]T. Komatsubara, M. Murakami, and E. Hirahara, J. Phys. Soc. Japan 18, 356 (1963).

[26]J. B. Merry, P. A. Fedders, and D. I. Bolef (unpublished).